IIETA International Information and Engineering Technology Association
Advancing the World of Information and Engineering

Mathematical Modelling of Engineering Problems
Vol. 11, No. 10, October, 2024, pp. 2657-2663
Journal homepage: http://iieta.org/journals/mmep

CFD Study of Prism-Shaped Vortex Generators' Impact Within a Coaxial Heat Exchanger

Mouhammad El Hassan[1*], Nikolay Bukharin[2], Nasser Alotaibi[1], Michel Matar[3], Hassan Hasan Assoum[3,4]

[1] Mechanical Engineering Department, Prince Mohammad Bin Fahd University, Al Khobar 34218, Saudi Arabia
[2] The Southern Alberta Institute of Technology (SAIT), Calgary AB T2M 0L4, Canada
[3] Mechanical Engineering Department, Beirut Arab University, Tripoli CRM7+3P2, Lebanon
[4] LASIE, University of Rochelle, La Rochelle 17000, France

Corresponding Author Email: melhassan@pmu.edu.sa

https://doi.org/10.18280/mmep.111007

Received: 13 August 2024
Revised: 5 October 2024
Accepted: 11 October 2024
Available online: 31 October 2024

Keywords:
coaxial heat exchanger, vortex generators, passive flow control, computational fluid dynamics (CFD), thermofluids

ABSTRACT

Heat exchangers are widely studied in energy and production processes. There are various techniques available to enhance the performance of heat exchangers, but in recent years, vortex generators have gained significant attention. Vortex generators (VGs) is a passive control method that can improve heat transfer if properly designed. Vortex generators achieve heat exchange enhancement by creating transverse, longitudinal, or normal twiddle flows, disrupting the flow field, and improving transport phenomena. The improvement in convective heat transfer coefficient is achieved by increasing fluid mixing, breaking down the thermal boundary layer, and improving mean velocity and temperature gradient. In this paper, a coaxial counter-flow heat exchanger was considered. Prism shape vortex generators were installed on the outer surface of the inner tube of the heat exchanger and resulting performance was compared to that of the same heat exchanger without vortex generators. RANS CFD study (SST k-ω turbulence model was used) demonstrated a 13% improvement in heat transfer rate when using a heat exchanger with vortex generators as compared to the case without VGs.

1. INTRODUCTION

The heat exchanger is a common element in various energy systems, and considerable effort is focused on enhancing its efficiency [1-4]. Several techniques exist to improve heat exchanger performance. Methods for heat transfer enhancement (HTE) have been studied both experimentally and numerically with the aim of conserving energy and minimizing the size and cost of heat exchange equipment. Among these methods, the passive approach stands out as a primary type, this method does not require any additional power input to improve heat transfer performance. Devices like vortex generators (VGs) play a crucial role in improving heat transfer efficiency and minimizing pressure drop in a passive way. Vortex generators boost heat exchanger's efficiency by creating transverse, longitudinal, or normal twiddle flows, disrupting the flow field, and improving transport phenomena. The enhancement of the convective heat transfer coefficient is accomplished by increasing fluid mixing, disrupting the thermal boundary layer, and improving the mean velocity and temperature gradient [5, 6].

There are various configurations of VGs, which are described in literature. Sreedhard and Varghese [7] explored the impact of various longitudinal fin arrangements on the overall heat transfer coefficient and heat transfer rate in a concentric double tube heat exchanger. The authors found that the highest heat transfer was observed in the case featuring external fins for the inner tube, exhibiting a 60.5% increase in the overall heat transfer coefficient compared to the base setup. This analysis was conducted under following assumptions: laminar fluid flow, hot water flowing through the inner tube, and cold water in the annular gap for all cases which were considered and aluminum was used for both the tube and fin material with a tube thickness of 0.001m. The inlet temperature of hot water was constant at 370K and the cold-water inlet was at 300K. ANSYS Fluent was used for all CFD simulations.

Li et al. [8] presented experimental measurements and comparison of the air-side pressure drops and overall heat transfer coefficients for a heat exchanger without fins; with and without a vortex generator cases were studied. It was demonstrated, that at dry conditions, a finless heat exchanger with a longitudinal vortex generator (LVG) exhibited a heat transfer performance approximately 40% lower than that of a fin-tube heat exchanger, while the pressure drop remained comparable. However, under wet conditions, the finless heat exchanger demonstrated equivalent heat transfer coefficients due to its exceptional drainage capabilities, with a lower pressure drop. In the case of frosting/defrosting conditions, the heat transfer coefficient was comparable, but the pressure drop was significantly reduced, reaching only 50 Pa at the conclusion of each frosting period.

To investigate the impacts of the angle of attack and aspect ratio on a winglet positioned near the leading edge of the fin

in a high-performance finned oval tube (FOT), Chen et al. [9] focused on evaluating heat transfer enhancement (HTE) and flow loss penalty (FLP) through three-dimensional flow and conjugate heat transfer analysis in a FOT. The calculations were conducted for a laminar flow (Re = 300) by employing the Navier-Stokes and energy equations, solved with a Finite Volume Method on body-fitted grids. The investigation included three angles of attack (β = 19°, 29°, and 34°) and two aspect ratios 1.5 and 2. The winglet with β = 19° and aspect ratio of 2 provided the best ratio of HTE to FLP.

Conducting experimental investigations, Chompookham et al. [10] aimed to analyze the impact of combined wedge ribs and winglet-type vortex generators (WVGs) on heat transfer and friction loss behaviors in turbulent airflow through a constant heat flux channel. Two configurations of wedge ribs, forming right triangles, were employed to induce reverse flow in the channel: one set pointing downstream and the other pointing upstream. Both types of ribs were arranged in in-line and staggered arrays within opposite channel walls. To promote longitudinal vortex flows through the test section, two pairs of WVGs with a 60° attack angle were installed at the channel inlet. The test channel, characterized by an aspect ratio (AR) of 10, a height (H) of 30 mm, a rib height (e/H) of 0.2, and a rib pitch (P/H) of 1.33, underwent airflow at varying Reynolds numbers based on the inlet hydraulic diameter, ranging from 5000 to 22,000. The use of combined ribs and WVGs resulted in a significant increase in both heat transfer rate and friction loss compared to a smooth channel. When combined with WVGs, the in-line wedge pointing downstream demonstrated the most significant improvement in both heat transfer rate and friction factor, while the staggered wedge pointing upstream exhibited the best thermal performance.

An experimental investigation of the heat transfer and flow friction characteristics within a solar air heater channel equipped with delta-winglet type vortex generators (DWs) was conducted by Skullong and Promvonge [11]. The experiments involved varying the airflow rate to achieve Reynolds numbers ranging from 5000 to 24000 in the test section, where uniform heat flux is applied to the upper channel wall. In the first scenario, DW pairs are installed solely at the entrance of the lower wall of the test channel (referred to as DW-E) to generate multiple Vortex flows at the entry. The study explored the impact of two transverse pitches (1 and 2) and three angles of attack angles (30°, 45°, and 60°) of the DW-E, considering its relative height b/H = 0.5 (half of the channel). In the second scenario, 30° DWs with three different relative heights (b/H 0.3, 0.4, and 0.5) were positioned exclusively on the upper wall (absorber plate, referred to as DW-A) of the test channel. The experimental results showed that, in the first case, the 60° DW-E at transverse pitch of 1 exhibited the highest heat transfer and friction factor, while the 30° DW-E at transverse pitch of 1 outperformed the other configurations. In the second case, the 30° DW-A at b/H = 0.5 demonstrated the highest heat transfer and friction factor, but the optimal thermal performance is observed at b/H = 0.4.

A plate-fin channel featuring rectangular wings functioning as transverse vortex generators was considered by Khoshvaght-Aliabadi et al. [12]. The heat transfer and fluid flow characteristics of this vortex-generator channel were analyzed through 3D CFD simulations. The impacts of seven effective geometrical parameters (namely, wings height, wings width, channel length, longitudinal wings pitch, transverse wings pitch, wings attach angle, and wings attack angle) were assessed for three conventional coolants (water, oil, and ethylene glycol) under laminar flow conditions. The inclusion of rectangular wings in the channel resulted in a 58.3% and 26.2% increase in the heat transfer performance of the plate-fin heat exchanger (PFHE) when compared to channels equipped with triangular and trapezoid wings, respectively. The values of heat transfer coefficient and pressure drop experience improvement with decreasing wings height, longitudinal wings pitch, and transverse wings pitch, as well as increasing wings width, channel length, and wings attack angle. Among the analyzed design parameters, wings height had the most significant impact on performance evaluation criteria and the values of heat transfer coefficient and pressure drop experienced improvement with decreasing wings height, longitudinal wings pitch, and transverse wings pitch, as well as increasing wings width, channel length, and wings attack angle.

The study conducted by Li et al. [13] was aimed to enhance heat transfer within the cross-corrugated triangular duct by introducing trapezoidal baffles into the flow channel. The investigation focused on assessing the impact of apex angle and baffle position on the heat and flow characteristics of the channel. Calculations were performed to obtain flow fields, velocity contours, and temperature contours. The numerical analysis involved examining friction factor (f), Nusselt number (Nu), and Performance Evaluation Criterion (PEC) for various channel structures. The presence of trapezoidal baffles introduced complexity to the flow channel compared to configurations without baffles. Across different apex angles, the friction factor (f) in flow channels with apex angles of 60° or 90° exhibited similar values, which were higher than those at 120°. This trend was also observed in the Nusselt number (Nu). Optimal values for f, Nu, and PEC were achieved when the baffles were positioned at the center of the upper half of the channel. Interestingly, for Reynolds numbers below 1000, the PEC value for the flow channel with a specific baffle position at an apex angle of 120° might be lower than that without baffles.

In the present study a simple coaxial heat exchanger was considered. Prism shape vortex generators were installed on the inner tube of a heat exchanger and performance was compared to performance of the same heat exchanger without vortex generators.

2. NUMERICAL MODEL

There are several models, which are used in order to describe the vortex dynamics and performance of heat exchangers. Delayed Detached Eddy Simulations were performed by Zhang et al. [14], using the k-ω-SST turbulence model to analyze the flow of pressurized helium gas at 8.0 MPa through cooling channels containing rib arrays on one wall. The simulations were conducted to study turbulent flow and heat transfer for arrays consisting of eight differently configured V-shaped and transverse ribs and dimples. RANS k-ω turbulence model was used by Aridi et al. [15] to study the effects of Vortex Generators (VGs) to enhance heat transfer inside the tube and annular. Tiwari et al. [16] found that RANS k-ε model was used to study thermofluidic characteristics of a novel heat exchanger design known as the Triple Tube Heat Exchanger. The comprehensive analysis was conducted while considering turbulent fluid-to-fluid heat transfer conditions.

In the present study RANS SST k-ω turbulence model was used, this model predicts well near-wall turbulence, which is

crucial when investigating the impact of vortex generators, it is essential to accurately represent the flow in the boundary layer zone. It can also handle well adverse pressure gradients and separation zones. Autodesk® CFD software was used to run simulations.

2.1 Geometry

Absolutely the same geometry was used in case of Heat Exchanger without vortex generators (Figure 1). The only difference was suppressed VGs.

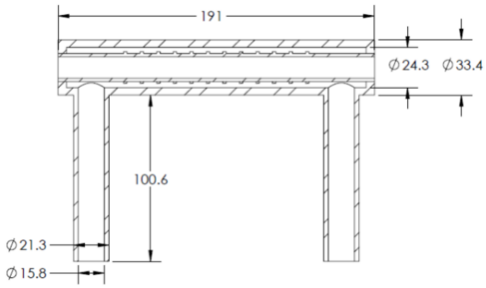

(a) Section view

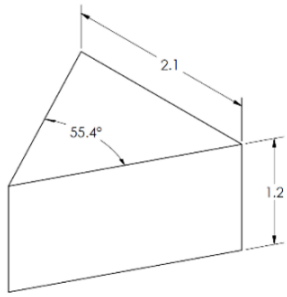

(b) Vortex generator

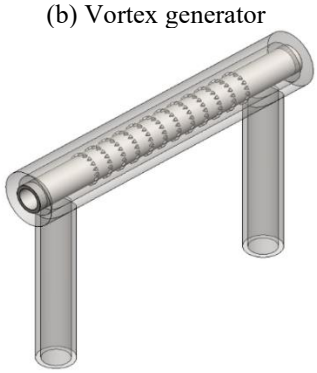

(c) Isometric view

Figure 1. Heat exchanger's geometry

2.2 Mesh and mesh independence

Autodesk® CFD utilizes tetrahedral mesh for 3D analysis. Mesh structure for VGs case is shown in Figure 2.

Mesh adaptation was used in this study. Mesh adaptation utilizes solution data to iteratively enhance the mesh definition, refining it for specific simulation requirements. This involves multiple simulation runs where each cycle builds upon the previous one, using the prior results to optimize the mesh. First, a baseline scenario with coarse mesh is run to given convergence. The mesh is refined based on velocity, pressure and temperature. The process repeats for each adaptation cycle. During each adaptation step, Autodesk® CFD evaluates the pressure, velocity, and temperature fields to determine how close the solution is to mesh independence. At the conclusion of each step, Autodesk® CFD reports the mesh independence status. Mesh independence was achieved after 4 adaptation steps at 2,483,810 of total elements with 1,816,381 of fluid Elements and 667,429 of solid elements without vortex generators and after 6 adaptation steps at 3,742,951 of total elements with 2,889,937 of fluid elements and with 853,014 of solid elements in case of vortex generators. The following mesh independence values were reported after last adaptation step: "Pressure: 99.98% Velocity: 100.00% Temperature: 100.00%". Each adaptation step was converged based on 1.0E-10 criteria. The residuals in Autodesk® CFD are defined as a measure of how well a solution vector X satisfies a matrix equation. The objective is to solve a matrix equation: AX = b. The residual vector, r is defined as, r = b - Ax. The L2 norm is typically used as it is a single value that characterizes the solution rather than a residual vector. Autodesk® CFD introduces two residuals Residual In which is the residual value of each degree of freedom, and is the measure of how much the quantity is changing. And Residual Out which is the value of the residual over the entire field after the last iteration. Residual In = L2_norm (AX - b) before the solver converges.

The Autodesk® CFD Solver forms A and b using the energy equation and uses the last value of X (temperature) to compute the L2_norm (AX - b). Residual Out = L2_norm (AX - b) after the solver has converged. The Solver outputs a solution vector X (temperature) and uses this to compute the residual going out of the solver. For a convergence criterion 1.0E-10: Residual Out = 1.0E-10×(Residual In). This specifies, that the outgoing residual is to be 10 orders of magnitude smaller than the incoming residual.

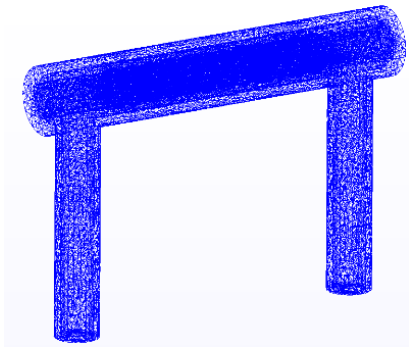

Figure 2. Mesh structure

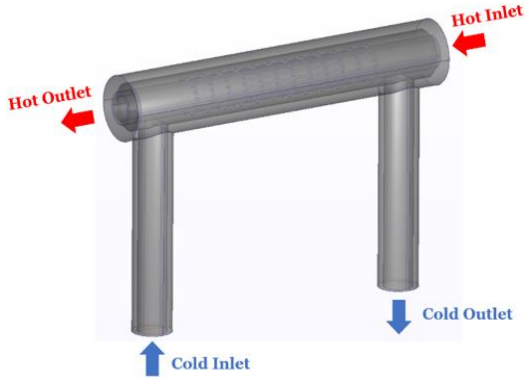

Figure 3. Inlets and outlets

2.3 Boundary conditions

Hot water was running through inner tube and cold water was running through the outside shell, countering hot fluid

flow (Figure 3). The material for both solids was set as stainless steel 316, steel conductivity was set as 0.163 W/cm-K. Temperature 36.7°C and volume flow rate 0.5 L/min was set on the hot water inlet and 23.6°C and 3.7 L/min was set on the cold water inlet. On both outlets atmospheric pressure was set as a boundary condition (0 Pa Gage). The outside shell wall is considered adiabatic. Same boundary conditions were used for the case without VGs.

2.4 Turbulence model equations

The SST k-ω turbulence model [17-20], is a two-equation eddy-viscosity model, which incorporates the shear stress transport (SST) formulation, and combines advantages from different modeling approaches. Specifically, the use of a k-ω formulation within the boundary layer's inner regions allows the model to be directly applicable down to the wall, including the viscous sub-layer. It can also function effectively as a Low-Re turbulence model without requiring additional damping functions. Additionally, the SST formulation effectively transitions to a k-ε behavior in the free-stream, addressing a common issue with k-ω models regarding sensitivity to inlet free-stream turbulence properties. SST k-omega Governing Equations for incompressible fluid:

Turbulence kinetic energy:

$$\frac{\partial k}{\partial t} + U_j \frac{\partial k}{\partial x_j} = P_k - \beta^* k\omega + \frac{\partial}{\partial x_j}\left[(\nu + \sigma_k \nu_T)\frac{\partial k}{\partial x_j}\right] \quad (1)$$

Specific dissipation rate:

$$\frac{\partial \omega}{\partial t} + U_j \frac{\partial \omega}{\partial x_j} = \alpha S^2 - \beta \omega^2 + \frac{\partial}{\partial x_j}\left[(\nu + \sigma_\omega \nu_T)\frac{\partial \omega}{\partial x_j}\right] + 2(1 - F_1)\sigma_{\omega 2}\frac{\partial k}{\partial x_i}\frac{\partial \omega}{\partial x_i} \quad (2)$$

Nematic eddy viscosity:

$$\nu_T = \frac{\alpha_1 k}{\max(\alpha_1 \omega, SF_2)} \quad (3)$$

Coefficients:

$$F_1 = tanh\left\{\left\{min\left[max\left(\frac{\sqrt{k}}{\beta^*\omega y}, \frac{500\nu}{y^2\omega}\right), \frac{4\sigma_{\omega 2}k}{CD_{k\omega}y^2}\right]\right\}^4\right\} \quad (4)$$

$$F_2 = tanh\left[\left[max\left(\frac{2\sqrt{k}}{\beta^*\omega y}, \frac{500\nu}{y^2\omega}\right)\right]^2\right] \quad (5)$$

$$P_k = min\left(\tau_{ij}\frac{\partial U_i}{\partial x_j}, 10\beta^*\omega y\right) \quad (6)$$

$$CD_{k\omega} = max\left(2\rho\sigma_{\omega 2}\frac{1}{\omega}\frac{\partial k}{\partial x_i}\frac{\partial \omega}{\partial x_i}, 10^{-10}\right) \quad (7)$$

Let $\Phi_1$represent any constant in the original k-ω model [21] and set Φ_2 represent any constant in standard k-ε model [22]. Φ represents the corresponding constant in SST k-ω model:

$$\Phi = F_1\Phi_1 + (1 - F_1)\Phi_2 \quad (8)$$

Final set of constants for SST k-ω model

$$\sigma_{k1} = 0.85, \sigma_{k2} = 1, \sigma_{\omega 1} = 0.5, \sigma_{\omega 2} = 0.856, \alpha_1 = \frac{5}{9}$$
$$\alpha_2 = 0.44, \beta_1 = \frac{3}{40}, \beta_2 = 0.0828, \beta^* = 0.09$$

Furthermore, continuity Eq. (9) and energy Eq. (10) were solved in a system.

$$\nabla \cdot u = 0 \quad (9)$$

For incompressible and subsonic flow, the energy equation is written in terms of static temperature.

$$\rho c_p \frac{\partial T}{\partial t} + \rho c_p u \frac{\partial T}{\partial x} + \rho c_p v \frac{\partial T}{\partial y} + \rho c_p w \frac{\partial T}{\partial z} = \frac{\partial}{\partial x}\left[K\frac{\partial T}{\partial x}\right] + \frac{\partial}{\partial y}\left[K\frac{\partial T}{\partial y}\right] + \frac{\partial}{\partial z}\left[K\frac{\partial T}{\partial z}\right] + q_V \quad (10)$$

3. RESULTS

Velocity plots in the midplane section can be seen in Figure 4.

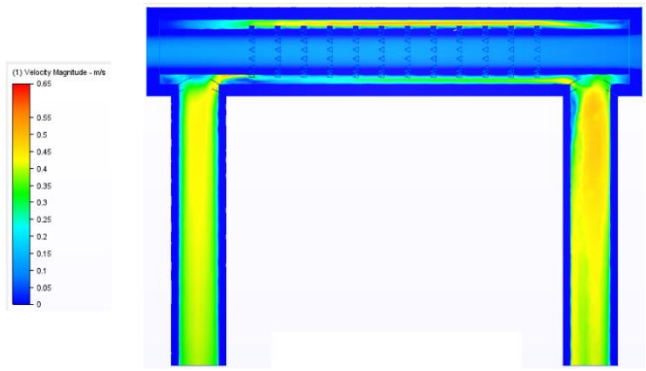

(a) Velocity: HE with vortex generators

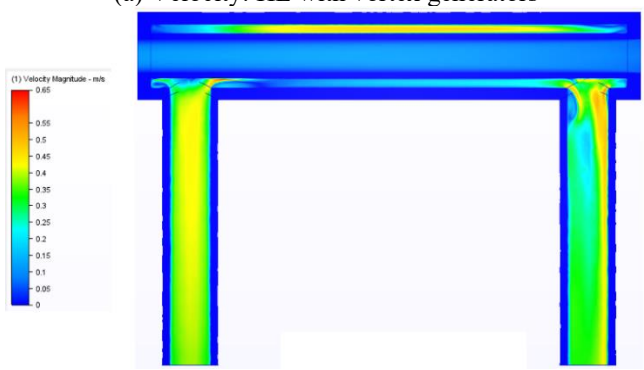

(b) Velocity: HE without vortex generators

Figure 4. Velocity in midplane section

It can be seen that water enters heat exchanger from the left and hits the internal tube generating a local recirculation zone. We can also observe recirculation region from the right, on the exit from the annular space, which is significantly reduced in case of heat exchanger with vortex generators. We can also observe elevated velocity at the exit from heat exchanger in case of vortex generators, contributing to better convective heat transfer, which can be seen in Figure 5.

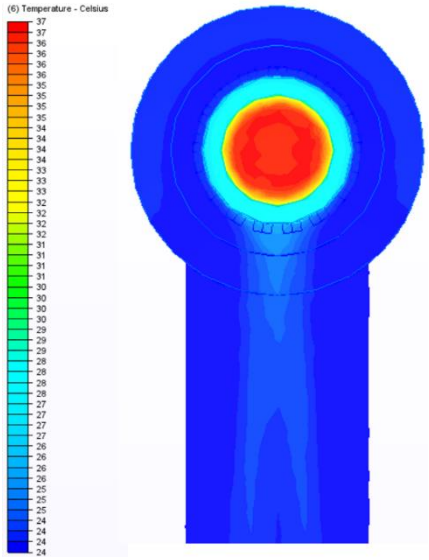

(a) With vortex generators

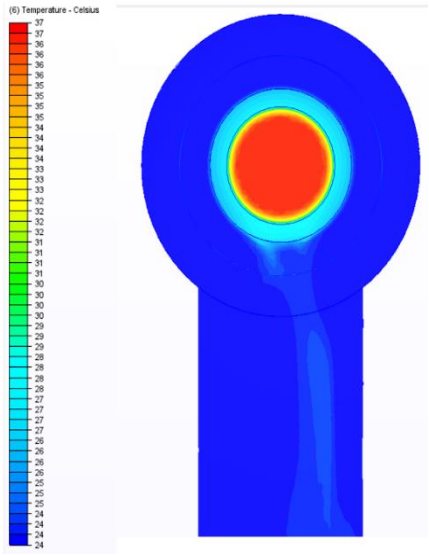

(b) Without vortex generators

Figure 5. Temperature distribution in the exit tube: Midplane section

Intense vorticity in the annular space (Figure 6), created by vortex generators (VGs), plays a crucial role in enhancing heat transfer in a heat exchanger. Vortices created by VGs are breaking down thermal boundary layers near the heat transfer surfaces, providing better heat transfer between the fluid and the heat exchange surface.

In addition to improving fluid-surface interaction, vorticity helps redistribute the fluid within the annular space. It prevents the formation of stagnant zones or hot spots by ensuring that all parts of the fluid receive adequate exposure to the heat transfer surface. This balanced fluid distribution optimizes heat transfer efficiency throughout the annular space.

Furthermore, intense vorticity reduces temperature differentials within the fluid. By promoting mixing and disrupting boundary layers, vortices help equalize temperatures across the annular space. This reduction in thermal gradients ensures that heat is transferred more evenly, leading to improved overall heat transfer performance.

As a result, we can observe slightly elevated temperatures on the outlet of cold-water tube and slightly reduced temperature on the outlet of hot water tube in case of heat exchanger with vortex generators in comparison to heat exchanger without vortex generators (Table 1).

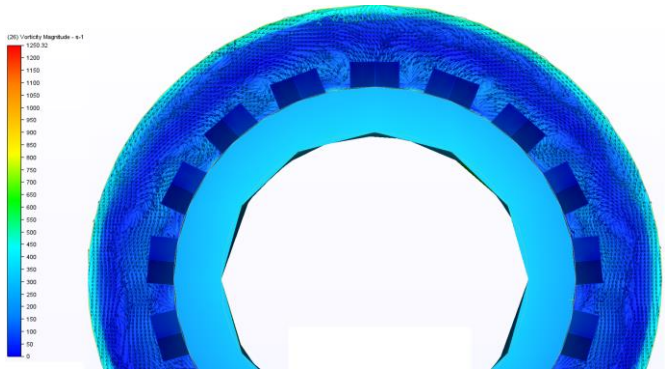

(a) Vorticity magnitude and velocity vectors behind VGs in annular space. Plane 6 from the left to right on (6c)

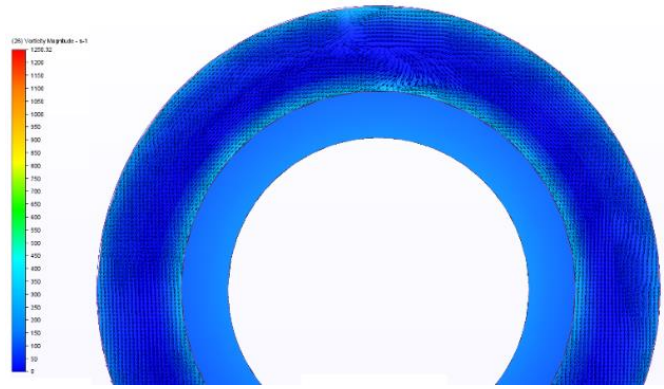

(b) Vorticity magnitude and velocity vectors in annular space without VGs. Plane 6 from the left to right on (6d)

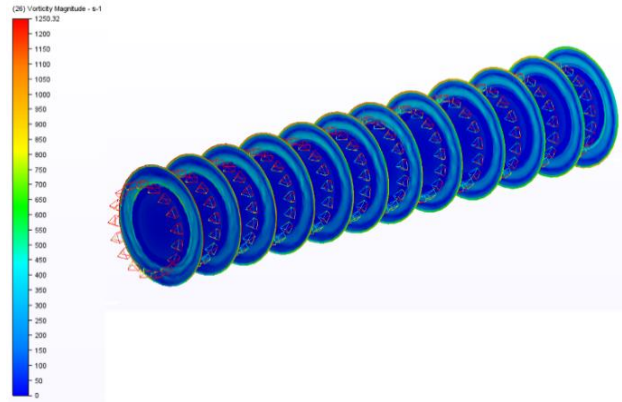

(c) Vorticity activity behind VGs along inner tube in annular space

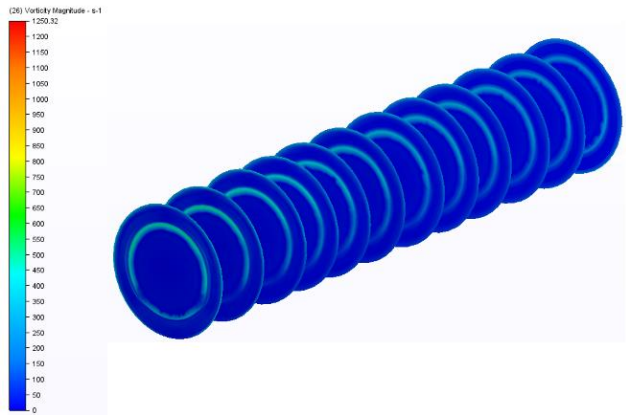

(d) Vorticity activity along inner tube in annular space without VGs

Figure 6. Vorticity

Table 1. Average temperatures and heat transfer rates

	With VGs	Without VGs
Cold Inlet Temperature	23.6oc	23.6oc
Cold Outlet Temperature	24.5oc	24.3oc
Hot Inlet Temperature	36.7oc	36.7oc
Hot Outlet Temperature	30.1oc	30.9oc
Heat Transfer Rate	230W	202W

That leads to 13.86% improvement in terms of heat transfer rate.

4. CONCLUSIONS

CFD study was performed to investigate the impact of prism shaped vortex generators, which were installed in coaxial heat exchanger's inner tube. The geometry was driven by simplicity and manufacturing costs for the future experimental validation.

The velocity plots in the midplane section, as shown in Figure 4, illustrates the impact of vortex generators (VGs) on fluid dynamics within the heat exchanger (HE). With VGs, the water entering from the left generates a local recirculation zone upon hitting the internal tube. Additionally, a recirculation region from the right, upon exit from the annular space, is reduced compared to the HE without VGs.

Figure 5 shows temperature distributions in the exit tube's midplane section. Heat Exchanger with VGs demonstrates elevated velocity at the exit, contributing to enhanced convective heat transfer. This is evident in the slightly elevated outlet temperature of the cold-water tube and slightly reduced outlet temperature of the hot water tube in the HE with VGs compared to without VGs, as indicated in Table 1.

The intense vorticity in the annular space, illustrated in Figure 6, is a key factor in this improvement. Vortices created by VGs play a critical role in breaking down thermal boundary layers near the heat transfer surfaces, providing better heat exchange between the fluid and the heat exchange surface. This intense vorticity also helps in redistributing the fluid within the annular space, preventing stagnant zones and optimizing heat transfer efficiency.

Overall, installed VGs lead to a 13.86% improvement in heat transfer rate compared to the HE without VGs. This improvement is attributed to the combined effects of reduced recirculation zones, enhanced convective heat transfer, and optimized fluid dynamics facilitated by intense vorticity in the annular space, showcasing the effectiveness of vortex generators in enhancing heat transfer performance.

REFERENCES

[1] Mahmoudinezhad, S., Sadi, M., Ghiasirad, H., Arabkoohsar, A. (2023). A comprehensive review on the current technologies and recent developments in high-temperature heat exchangers. Renewable and Sustainable Energy Reviews, 183: 113467. https://doi.org/10.1016/j.rser.2023.113467

[2] Patel, A. (2023). Heat exchangers in industrial applications: Efficiency and optimization strategies. International Journal of Engineering Research & Technology, 12(9): 3.

[3] Al-Barqi, A.S., Bukharin, N., Zazoum, B., El Hassan, M. (2022). Design of a 100 MW concentrated solar power Linear Fresnel plant in Riyadh, Saudi Arabia: A comparison between molten salt and liquid sodium thermal energy storage. Energy Reports, 8: 697-704. https://doi.org/10.1016/j.egyr.2022.08.055

[4] He, Y., Jia, M., Li, X., Yang, Z., Song, R. (2021). Performance analysis of coaxial heat exchanger and heat-carrier fluid in medium-deep geothermal energy development. Renewable Energy, 168: 938-959. https://doi.org/10.1016/j.renene.2020.12.109

[5] Khoshvaght-Aliabadi, M., Sartipzadeh, O., Alizadeh, A. (2015). An experimental study on vortex-generator insert with different arrangements of delta-winglets. Energy, 82: 629-639. https://doi.org/10.1016/j.energy.2015.01.072

[6] Awais, M., Bhuiyan, A.A. (2018). Heat transfer enhancement using different types of vortex generators (VGs): A review on experimental and numerical activities. Thermal Science and Engineering Progress, 5: 524-545. https://doi.org/10.1016/j.tsep.2018.02.007

[7] Sreedhard, N., Varghese, G. (2017). Analysis of longitudinal fin patterns in a concentric double tube heat exchanger using LMTD and CFD techniques. International Journal of Applied Engineering Research, 12(17): 6471-6479.

[8] Li, J., Dang, C., Hihara, E. (2019). Heat transfer enhancement in a parallel, finless heat exchanger using a longitudinal vortex generator, Part B: Experimental investigation on the performance of finless and fin-tube heat exchangers. International Journal of Heat and Mass Transfer, 128: 66-75. https://doi.org/10.1016/j.ijheatmasstransfer.2018.06.048

[9] Chen, Y., Fiebig, M., Mitra, N.K. (1998). Conjugate heat transfer of a finned oval tube with a punched longitudinal vortex generator in form of a delta winglet—parametric investigations of the winglet. International Journal of Heat and Mass Transfer, 41(23): 3961-3978. https://doi.org/10.1016/S0017-9310(98)00076-3

[10] Chompookham, T., Thianpong, C., Kwankaomeng, S., Promvonge, P. (2010). Heat transfer augmentation in a wedge-ribbed channel using winglet vortex generators. International Communications in Heat and Mass Transfer, 37(2): 163-169. https://doi.org/10.1016/j.icheatmasstransfer.2009.09.012

[11] Skullong, S., Promvonge, P. (2014). Experimental investigation on turbulent convection in solar air heater channel fitted with delta winglet vortex generator. Chinese Journal of Chemical Engineering, 22(1): 1-10. https://doi.org/10.1016/s1004-9541(14)60030-6

[12] Khoshvaght-Aliabadi, M., Zangouei, S., Hormozi, F. (2015). Performance of a plate-fin heat exchanger with vortex-generator channels: 3D-CFD simulation and experimental validation. International Journal of Thermal Sciences, 88: 180-192. https://doi.org/10.1016/j.ijthermalsci.2014.10.001

[13] Li, Z.X., Sun, S.Q., Wang, C., Liang, C.H., et al. (2022). The effect of trapezoidal baffles on heat and flow characteristics of a cross-corrugated triangular duct. Case Studies in Thermal Engineering, 33: 101903. https://doi.org/10.1016/j.csite.2022.101903

[14] Zhang, P., Rao, Y., Xie, Y., Zhang, M. (2021). Turbulent flow structure and heat transfer mechanisms over surface vortex structures of micro V-shaped ribs and dimples. International Journal of Heat and Mass Transfer, 178:

121611. https://doi.org/10.1016/j.ijheatmasstransfer.2021.121611
[15] Aridi, R., Ali, S., Lemenand, T., Faraj, J., Khaled, M. (2022). CFD analysis on the spatial effect of vortex generators in concentric tube heat exchangers–A comparative study. International Journal of Thermofluids, 16: 100247. https://doi.org/10.1016/j.ijft.2022.100247
[16] Tiwari, A.K., Javed, S., Oztop, H.F., Said, Z., Pandya, N.S. (2021). Experimental and numerical investigation on the thermal performance of triple tube heat exchanger equipped with different inserts with WO3/water nanofluid under turbulent condition. International Journal of Thermal Sciences, 164: 106861. https://doi.org/10.1016/j.ijthermalsci.2021.106861
[17] Menter, F. (1993). Zonal two equation kw turbulence models for aerodynamic flows. In 23rd Fluid Dynamics, Plasmadynamics, and Lasers Conference, Orlando, USA, p. AIAA-93-2906. https://doi.org/10.2514/6.1993-2906
[18] Menter, F.R. (1994). Two-equation eddy-viscosity turbulence models for engineering applications. AIAA Journal, 32(8): 1598-1605. https://doi.org/10.2514/3.12149
[19] El Hassan, M., Bukharin, N. (2019). Numerical investigation of the flow dynamics inside single fluid and binary fluid ejectors. Journal of Physics: Conference Series, 1276(1): 012012. https://doi.org/10.1088/1742-6596/1276/1/012012
[20] Widiawaty, C.D., Siswantara, A.I., Gunadi, G.G.R., Pujowidodo, H., Syafei, M.H.G. (2020). A CFD simulation and experimental study: Predicting heat transfer performance using SST k-ω turbulence model. IOP Conference Series: Materials Science and Engineering, 909(1): 012004. https://doi.org/10.1088/1757-899X/909/1/012004
[21] Wilcox, D.C. (1988). Reassessment of the scale-determining equation for advanced turbulence models. AIAA Journal, 26(11): 1299-1310. https://doi.org/10.2514/3.10041
[22] Jones, W.P., Launder, B. (1973). The calculation of low-Reynolds-number phenomena with a two-equation model of turbulence. International Journal of Heat and Mass Transfer, 16(6): 1119-1130. https://doi.org/10.1016/0017-9310(73)90125-7

NOMENCLATURE

c_p	specific heat, J. kg^{-1}. K^{-1}
$CD_{k\omega}$	cross-diffusion term
F_1, F_2	blending functions
k	turbulence kinetic energy
K	thermal conductivity, W.m^{-1}. K^{-1}
Nu	Nusselt number
P_k	production cross-diffusion term
Re	Reynolds number
S	strain rate magnitude
T	temperature
u	velocity vector
U	mean flow velocity

Greek symbols

α_1, α_2	constants for SST k-ω model
β_2, β^*	constants for SST k-ω model
σ_{k1}, σ_{k2}, $\sigma_{\omega1}$, $\sigma_{\omega2}$	constants for SST k-ω model
ν_T	kinematic eddy viscosity
ρ	density
ω	specific dissipation rate
Φ_1, Φ_2, Φ	sets of constants in k-ω and k-ε turbulence models